



# Microstructural Characteristics and Mechanical Properties of CNT/Ni Coated CNT–Dispersed Al Alloys Produced by High Energy Ball Milling and Hot Extrusion

N. S. Anas<sup>1,2</sup> · M. Ramakrishna<sup>1</sup> · R. Vijay<sup>1</sup>

Received: 17 February 2019 / Accepted: 7 June 2019 / Published online: 21 June 2019  
© The Korean Institute of Metals and Materials 2019

## Abstract

The effect of dispersion of carbon nanotubes (CNT) and Ni coated CNT in Al alloy (AA) on the evolution of microstructure and resultant mechanical properties are investigated. Al alloy (Al–4.4Cu–0.5Mg), Al alloy–CNT (AC) and Al alloy–Ni coated CNT (ANC) composites were produced from elemental powders by mechanical milling (MM) followed by hot extrusion. Unlike CNT–containing Al or Al alloy milled powders,  $\text{Al}_4\text{C}_3$  phase formed during milling of ANC powder. The formation of  $\text{Al}_4\text{C}_3$  is due to the dissolution of Ni present on CNT surface in Al alloy during MM, thereby, creating defects on CNT that promoted  $\text{Al}_4\text{C}_3$  formation. AC and ANC samples exhibited larger size and lower number density of  $\theta'$  precipitates when compared to AA. The larger size of  $\theta'$  precipitates is due to the presence of ultra-fine grains, reduced quenched-in vacancies and higher dislocation density that promoted the nucleation resulting in enhanced precipitation and growth kinetics. The strengths of AC and ANC samples are higher when compared to CNT-free AA, and ANC exhibited highest yield strength of 567 MPa. However, the ductility of ANC sample is not improved due to the presence of  $\text{Al}_7\text{Cu}_4\text{Ni}$  phase, which promoted crack initiation.

**Keywords** Aluminium matrix composites · Mechanical alloying · Multi-walled carbon nanotubes · Structure–property correlation

## 1 Introduction

The need to produce lighter, stronger and stiffer materials has been a continuous prerequisite for aerospace and automotive industries; not only for improving the fuel efficiency of the engines but also for reducing the exhaust gas emissions. Amongst light weight materials, Al alloys have always been the first choice due to good machinability, ductility, thermal conductivity, formability etc. [1, 2]. However, at higher homologous temperatures, the performance of Al alloys is poor owing to the deterioration of strength and stiffness [1]. Various methodologies to integrate the characteristics of

Al alloys, and the superior stiffness and strength levels of ceramic particles, whiskers and graphite derived carbons etc., led to the development of Al alloy matrix composites (AMCs) [3]. For instance,  $\text{Al}_2\text{O}_3$  dispersed Al alloy, also known as sintered aluminium product, SAP, is one such material which was proven to maintain substantial strength levels even up to 300 °C [4, 5].

Presently, carbon nanotubes (CNT) are being considered as one of the potential reinforcements due to the intrinsic higher mechanical properties (UTS  $\approx$  100 GPa and  $E \approx$  1 TPa) [3, 6]. The reported significant improvement in strength, stiffness and wear resistance of CNT reinforced–AMCs was attributed to the dispersion and grain boundary strengthening, and the load transfer mechanism by CNT [7–11]. However, the stiffness and strength levels attained in CNT–reinforced AMCs have not reached up to that of inherent properties of CNT. This shortcoming is due to the inability of processing methods: (1) to uniformly disperse CNT in the Al matrix, (2) to provide a good Al matrix–CNT interfacial bonding and (3) to avoid the formation of detrimental phases at elevated temperatures [3].

✉ N. S. Anas  
anastzns@gmail.com

<sup>1</sup> International Advanced Research Centre for Powder Metallurgy and New Materials (ARCI), Balapur P O., Hyderabad 500005, India

<sup>2</sup> School of Engineering Sciences and Technology, University of Hyderabad, Gachibowli, Hyderabad 500046, India

Appropriate methods for CNT dispersion and subsequent consolidation are essential in addressing these issues. The limitation of conventional melting–solidification process to overcome the above challenges gave way to the production of Al–CNT composites by powder metallurgy (P/M) [1].

Amongst various processing methods in P/M, mechanical milling (MM) of elemental or pre–alloyed powders with CNT is being considered as one of the efficient techniques to disperse CNT in Al matrix. The refinement of matrix grains that occurs due to MM also results in strengthening of the material. The consolidation of CNT–reinforced AMCs including hot isostatic pressing, cold pressing, spark plasma sintering, hot extrusion etc. have already been used by many researchers [7–11]. It is reported that plastic deformation during hot extrusion helps in spreading any agglomerated or entangled CNT [12], and hence it is used in this study.

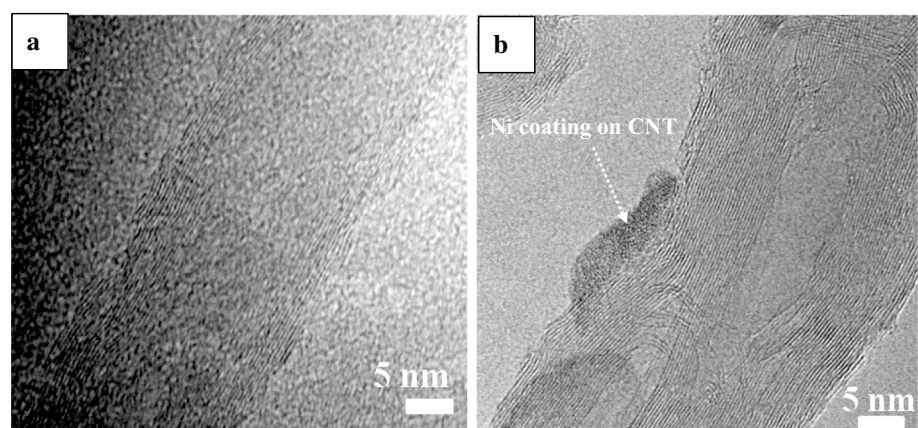
Although CNT reinforced–AMCs exhibited superior strength than the corresponding base material, a concurrent decrease in ductility was also observed. The reduction in ductility of these materials is due to the poor interfacial bonding between Al matrix and CNT. One of the methodologies to address this issue is to coat the surface of CNT with Ni or Cu which have good wettability with CNTs and also benign to Al matrix [13–15]. Jagannatham et al. compared the Cu coated CNT reinforced Al composite with that of uncoated CNT–Al composite [14]. These composites with 0–2 wt% Cu coated CNT content were produced by ball milling for 1 h at 300 rpm and consolidated by spark plasma sintering. An increase of about 220% of compressive proof strength in 2 wt% CNT dispersed–Al composites as compared to Al was ascribed to the efficient load transfer mechanism due to the improved interfacial bonding between Al and CNT. Similar enhanced strength levels were also reported by Maqbool et al. [15] who fabricated Al–(0–1 wt%) Cu coated CNT composites by ultrasonic mixing, mechanical milling followed by hot rolling. However, with the dispersion of uncoated or Cu coated CNT in Al matrix, it was found that the ductility declined further in Cu coated CNT dispersed

composites than that of uncoated ones for the same weight fraction of CNT. Carvalho et al. [16, 17] studied Al–Si alloy–Ni coated CNT composites produced by ball milling at 40 rpm for 6 days and subsequent hot vacuum pressing at 550 °C. The enhancement in strength of the composites was proposed to be due to the formation of Al<sub>3</sub>Ni at the interface, even though no qualitative information regarding this phase formation was provided [17]. Hence, in the current study Ni coated CNT was selected as reinforcement material to produce Al alloy matrix composites and to understand the process dependent structure–property correlations of Al alloy–CNT/Ni coated CNT composites produced by MM of elemental powders and consolidation by hot extrusion.

## 2 Materials and Methods

Specifications of commercial Al, Cu and Mg powders used in the study are given elsewhere [18]. Multi–walled carbon nanotubes (CNT), having diameter: 20–30 nm, length: 1 µm and purity: 98%, were procured from Bayers materials science, Germany, and nickel coated multi walled carbon nanotubes (Ni coated CNT), having diameter: 50–80 nm, length: 10–20 µm and purity: 98%, were obtained from US Nanomaterials, Inc., USA. TEM images of as–received CNT and Ni coated CNT, as shown in Fig. 1a, b, clearly displayed the walls of both the carbon nanotubes and coating of Ni on the surface of CNT. Al alloy, Al alloy–CNT and/or Ni coated CNT composite powders were produced in two stages: (1) Al master alloy (Al–22Cu–0.5Mg) was prepared by milling Al, Cu and Mg powders in Fritsch planetary mill for 20 h by using ethylene glycol as a process control agent (PCA), (2) Master alloy blended with adequate quantities of powders of Al, Mg, CNT and Ni coated CNT to form Al alloy (Al–4.4Cu–0.5Mg), Al alloy–1.5 CNT and Al alloy–1.5 Ni coated CNT composite powders and milled in Zoz Simoloyer for 4 h under argon atmosphere using methanol (0.5 wt%) as PCA [19]. Vacuum annealing ( $5 \times 10^{-5}$  kPa)

**Fig. 1** TEM images showing the morphologies of as–received: **a** Multi walled carbon nanotubes (CNT) and **b** Ni coated multi walled carbon nanotubes (Ni coated CNT)



of milled powders was carried out at 500 °C for 2 h, and the annealed powders were subsequently filled in Al cans and sealed at 250 °C under a vacuum level of  $4 \times 10^{-6}$  kPa. The powder filled cans were hot pressed at 500 °C at a pressure of 350 MPa, followed by extrusion at 500 °C under a pressure of 510 MPa, with an extrusion ratio of 16. Solution treatment of extruded rods was carried out at 500 °C, 2 h, water quenched and peak aged at 150 °C, 4 h according to the pre-optimized condition mentioned in our earlier work [18].

For the ease of understanding, Al alloy, Al alloy–CNT and Al alloy–Ni coated CNT composites are termed as AA, AC and ANC, respectively and their compositions are presented in Table 1. Raman spectroscopy was carried out using Horiba LabRam with an excitation wavelength of 531.6 nm. Morphology of milled powders were imaged using scanning electron microscope (SEM, S–3400N, Hitachi), while phase analysis and particle size measurements were carried out using X-ray diffractometer (XRD, Bruker's D8 advance AXS diffractometer) and dynamic light scattering (MasterSizer 2000, Malvern) respectively. Microstructures of hot pressed and extruded samples were captured using Olympus DSX510 opto-digital microscope, whereas transmission electron microscope (TEM, FEI Tecnai G<sup>2</sup>) operated at acceleration voltage of 200 kV was used for characterizing the microstructure of bulk samples in peakaged condition. TEM samples were prepared by mechanical grinding to 100  $\mu\text{m}$ , followed by dimpling up to 30  $\mu\text{m}$  and ion milling with argon at 4 kV till perforation. Dislocation density ( $\rho$ ) of the samples in peakaged condition was estimated using the expression given below [20]:

$$\rho = \frac{2\sqrt{3} \cdot \varepsilon}{d \cdot b} \quad (1)$$

where  $\varepsilon$  is the microstrain,  $d$  is the crystallite size and  $b$  is the burgers vector.  $\varepsilon$  can be found out using XRD peak broadening method proposed by Williamson and Hall [21], as given in Eq. 2:

$$\beta \cdot \cos\alpha = \lambda/d + \varepsilon \cdot \sin\alpha \quad (2)$$

where  $\alpha$  is the Bragg's diffraction angle,  $\beta$  is the net full width of the XRD peak considered at half-maximum intensity (FWHM) after deducting the FWHM of instrumental broadening and  $\lambda$  is the wavelength of X-rays. The average

size and distributions of grains and  $\theta'$  precipitates of all the samples were estimated from a minimum of 5 TEM images captured from regions taken at random. For this quantification, more than 300 grains and 150 precipitates were taken into account and images were processed by utilizing the 'Image analysis' software. The volume fraction of  $\theta'$  precipitates was estimated using the expression given below [22]:

$$f_v = \sum_{i=1}^n \frac{\left(\frac{T_i}{0.8285 \cdot l_i + T_i}\right) \cdot \left(\frac{1}{4} \cdot \pi \cdot l_i^2 \cdot T_i\right) + \left(\frac{0.8285 \cdot l_i}{0.8285 \cdot l_i + T_i}\right) \cdot (0.8137 \cdot l_i^2 \cdot t_i)}{\text{area} \cdot (0.8285 \cdot l_i + T_i)} \quad (3)$$

where  $n$  is the number of the  $\theta'$  precipitates in the area of observation,  $T_i$  is the thickness of TEM sample (90 nm, measured using CBED technique),  $l_i$  and  $t_i$  are the length and thickness of  $i$ th  $\theta'$  precipitate. Vickers hardness tester (Walter UHL, VMHT) was used to measure hardness of samples with a load of 500 g and the average value obtained from at least 15 indentations is reported. Tensile properties (Young's modulus, percentage strain to failure, and yield and ultimate tensile strengths) were evaluated at room temperature with a strain rate of  $5.5 \times 10^{-4} \text{ s}^{-1}$  according to the ASTM E8M standard using universal testing machine Instron 5500R. Fractography of samples was carried out using SEM.

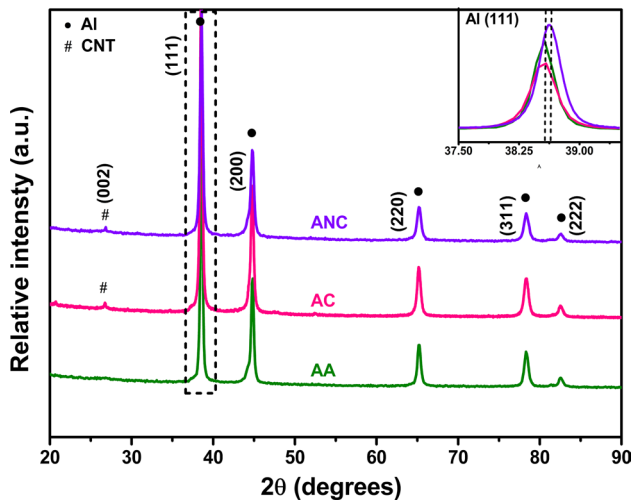
## 3 Results and Discussion

### 3.1 Characterization of Milled Powders

XRD patterns of milled powders of AA, AC and ANC are given in Fig. 2. The Al peaks corresponding to (111), (200), (220), (311) and (222) lattice planes are observed in all the samples. However, in addition to Al, a minor peak is also identified at  $26^\circ$  in AC and ANC samples, which corresponds to the characteristic peak of (002) lattice plane of graphite indicating the presence of carbon nanotubes in both the samples. No peak associated with Cu or Mg is found in the XRD patterns, which suggests the dissolution of these elements in Al lattice. Apart from that, the high intensity Al peak of ANC sample (shown as an inset of Fig. 2) exhibited a little peak-shift towards higher side [23, 24] and hence, it is inferred that Ni atoms also gone into the solid solution of Al during MM.

**Table 1** Nomenclature and composition of Al alloy–CNT composites (wt%)

Sample ID	Name	Cu	Mg	CNT	Ni	Al
AA	Al alloy	4.4	0.5	0	—	Rem.
AC	Al alloy–CNT composite	4.4	0.5	1.5	—	Rem.
ANC	Al alloy–Ni coated CNT composite	4.4	0.5	1.5	2.25	Rem.



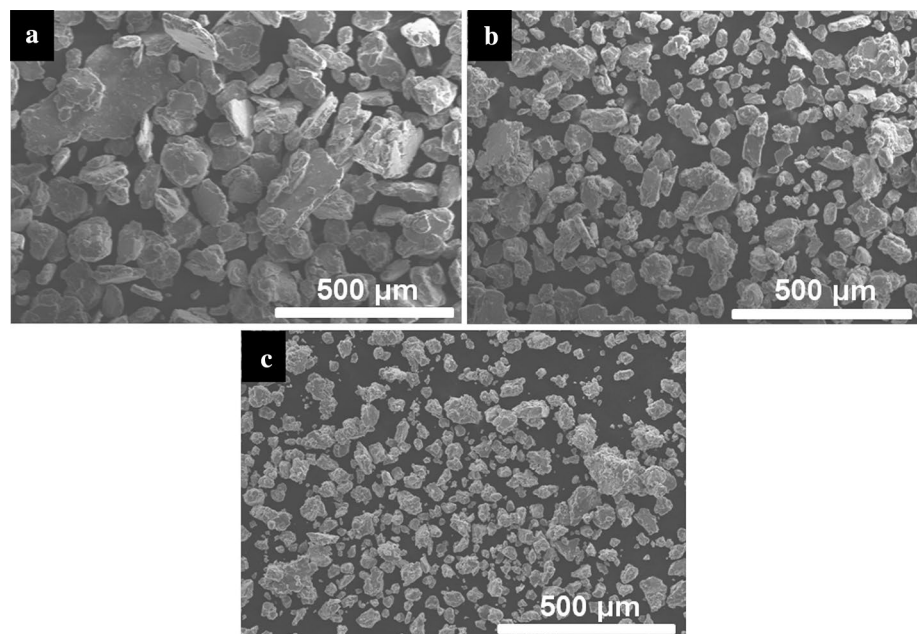
**Fig. 2** XRD patterns of milled powders of AA, AC and ANC samples. The maximum intensity Al (111) peaks are shown as an inset

Figure 3 shows the morphology of milled powders of AA, AC and ANC. Particles of both rounded and flake-like shapes were observed in all the samples. However, the particle size of AA reduced with dispersion of CNT/Ni coated CNT, and the average particle size for AA, AC and ANC samples is estimated to be 64, 52 and 41  $\mu\text{m}$  respectively. It is established that during mechanical milling, Al and Al alloy powder particles undergo cycles of plastic deformation, strain saturation, fracturing and cold welding leading to a steady state particle size that represents the dynamic equilibrium of above mentioned events [4, 25]. It is also reported that the process control agent (PCA) effectively

reduces the particle size of milled powders by decelerating the cold welding [26]. So, it can be inferred that the presence of CNT and Ni coated CNT in the respective AC and ANC samples act as PCA thereby reducing the particle size of milled powder. The relatively lower particle size in ANC as compared to AC sample can be attributed to the enhanced work hardening of powders due to the possible dissolution of Ni in Al during MM, thereby favouring the fracture [27].

Raman spectroscopy of milled powders of AA, AC and ANC was also carried out to find out the existence of CNT in Al alloy matrix after 4 h of milling and the spectra are shown in Fig. 4. Raman spectra of as-received CNT and Ni coated CNT are also included in the same figure for reference. All the signature peaks i.e., *D* band (vibrations due to defects), *G* band (vibrations due to graphitic structure) and *G'* band (overtone of *D* and *G* bands) were observed in both CNT and Ni coated CNT. This implies that both the carbon nanotubes have some defects in the as-received condition itself. However, Ni coated CNT exhibited lower intensity *D* band, higher intensity *G* and *G'* bands, than that of CNT. Also, the lower  $I_D/I_G$  ratio of 0.73 for Ni coated CNT as compared to that of 1.39 for CNT, suggests the presence of more defects in CNT confirming the relatively good quality of Ni coated CNT. Since there is no Raman active phase present, milled powders of AA sample did not exhibit any peaks in its Raman spectrum. Yet, in the case of AC and ANC samples after milling, the intensity of *D* band, and correspondingly the  $I_D/I_G$  ratio of AC and ANC samples increased, due to the structural damages imparted to both CNT and Ni coated CNT because of high kinetic impacts. AC and ANC samples displayed only *D* and *G*-bands but not *G'*. The absence of *G'* band might be due to either the lower weight fraction of

**Fig. 3** Morphologies of milled powders of: **a** AA, **b** AC and **c** ANC



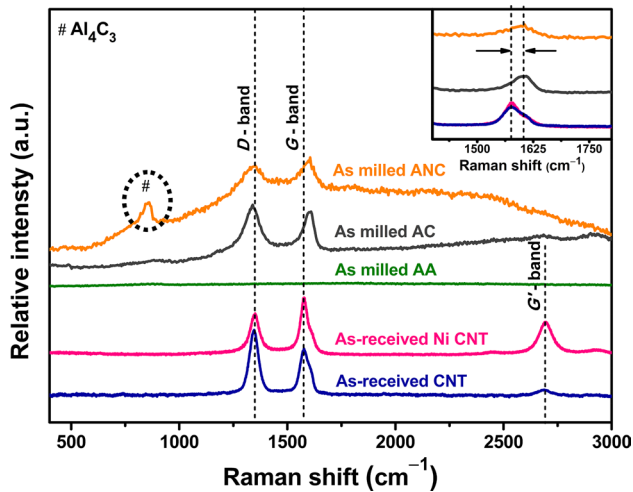


**Fig. 4** Raman spectra of as-milled powders of AA, AC and ANC samples are compared with as-received CNT and Ni coated CNT. The dotted circle indicates the presence of  $\text{Al}_4\text{C}_3$  phase in ANC. The shift in  $G$ -band of milled powders with respect to as-received powders is also shown as an inset

CNT present in AC and ANC samples or the detection limit of Raman spectroscopy employed in this study. Also, it is noted that the shifting of  $G$ -band ( $\sim 31 \text{ cm}^{-1}$ ) to higher wave number in AC and ANC samples when compared to respective as-received CNT and Ni coated CNT was observed to be identical (inset of Fig. 4) in both the samples. This shifting is due to the infiltration of Al atoms into CNT/Ni coated CNT as well as the residual stresses generated in both the CNT and Ni coated CNT during milling [18].

However, contrary to the reported literature on the milled powders of CNT-reinforced Al and Al alloy composites [27–32],  $\text{Al}_4\text{C}_3$  phase was observed in the milled powder

of ANC sample (Fig. 4). Raman shift at about  $800 \text{ cm}^{-1}$  is related to the vibrations corresponding to  $\text{Al}_4\text{C}_3$  phase. It is known that carbides are not formed until the crystalline nature of CNT is heavily destroyed during processing of Al or Al alloy–CNT composites [33, 34]. It is also reported that the formation of  $\text{Al}_4\text{C}_3$  phase is due to the chemical reaction between CNT (having damages caused by MM) and the neighbouring Al or Al alloy matrix that takes place at a higher heat treatment/consolidation temperature ( $400\text{--}550 \text{ }^\circ\text{C}$ ) [28, 33]. However, in the context of the present study, the formation of  $\text{Al}_4\text{C}_3$  phase in ANC sample can be postulated as follows: During MM of ANC sample, Ni atoms (in Ni coated CNT) undergo dissolution in Al (Fig. 2) leaving behind defects on the surface of CNT. The concurrent localized rise in temperature during MM aided the formation of  $\text{Al}_4\text{C}_3$  phase at the defect–Al matrix interface. The drastic reduction of  $G$ -band in ANC milled powder from the as-received Ni coated CNT also confirms the possible increase in the defect density of CNT. So it can be inferred that the structural integrity of CNT during processing stages has a major role for the modification and subsequent conversion of CNT to  $\text{Al}_4\text{C}_3$  phase.

### 3.2 Characterization of Consolidated Samples

Raman spectra obtained from AC and ANC samples in hot pressed, hot extruded and peakaged conditions are shown in Fig. 5a–b. In addition to  $D$  and  $G$ -bands,  $\text{Al}_4\text{C}_3$  phase formation is observed in both the samples irrespective of the conditions. The  $I_D/I_G$  ratio obtained on hot pressed, hot extruded and peakaged samples is found to be comparable at all the aforementioned processing stages of AC and ANC samples (Table 2). This suggests that the structural integrity of CNT after milled condition is retained even after the

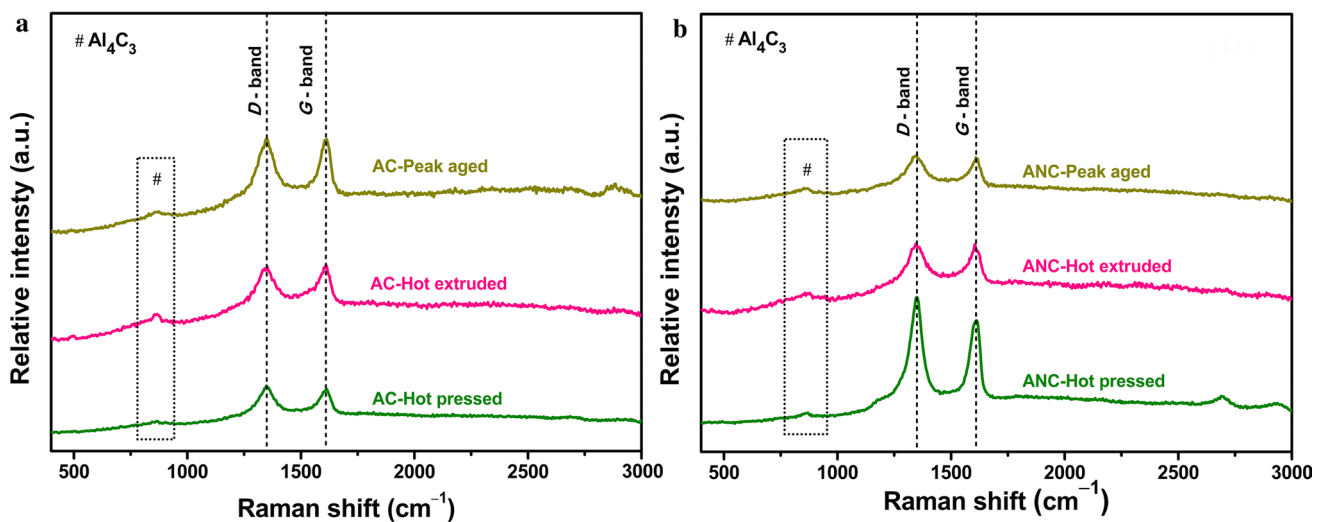


**Fig. 5** Raman spectra of: **a** AC and **b** ANC samples at different stages of processing

**Table 2** Estimated  $I_D/I_G$  ratio of AC and ANC samples

Sample	Hot pressed	Hot extruded	Peak aged
AC	1.1	1.01	1.01
ANC	1.1	0.97	0.99

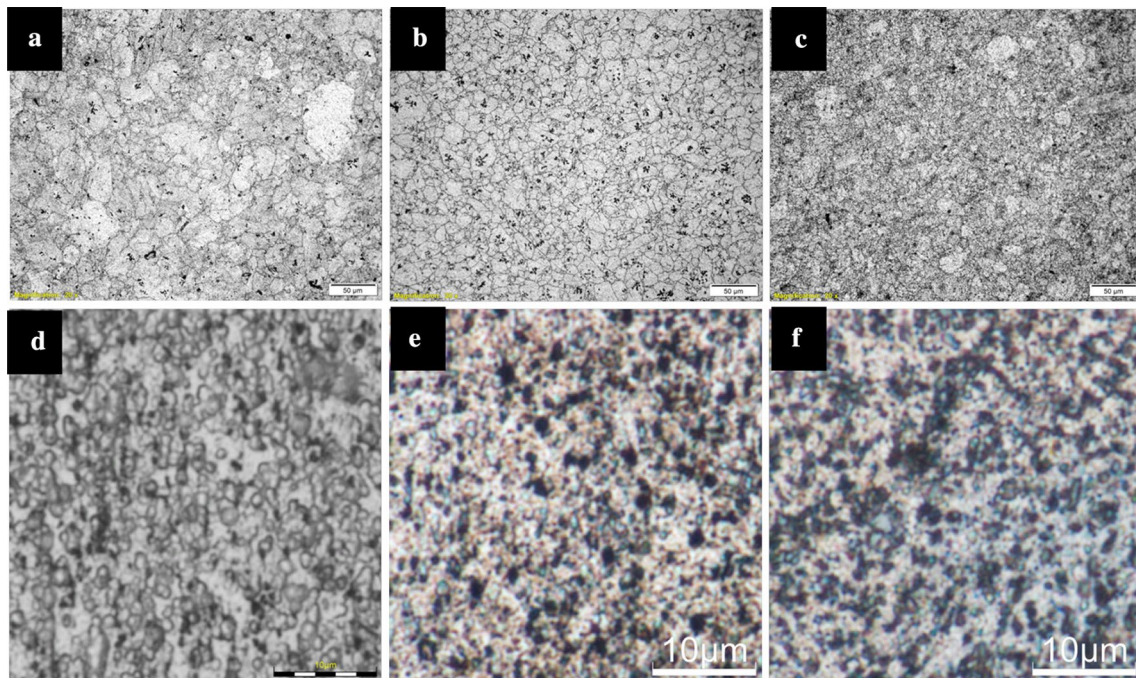
plastic deformation during pressing and extrusion, and the thermal strain generated during solution and peak ageing treatments. Also, the  $Al_4C_3$  phase formed during milling of ANC sample is preserved in the subsequent processing stages as well.

Optical micrographs of AA, AC and ANC samples after hot pressing are shown in Fig. 6a–c. It is observed that the grain size decreased in the order of  $AA > AC > ANC$  and the average grain size is found to be  $34.3 \pm 7.4$ ,  $15.7 \pm 5.2$ ,  $9.5 \pm 4.8$   $\mu m$  respectively. The microstructures of longitudinally-sectioned AA, AC and ANC samples after extrusion are shown in Fig. 6d–f. It is evident that the grains of all samples were further refined by an order of magnitude after hot extrusion [35]. This can be attributed to dynamic recrystallisation that occurs during plastic deformation at higher working temperatures [36, 37]. The average grain size of extruded AA, AC and ANC samples follows in the same order as that of hot pressed condition and the values are  $1.29 \pm 0.36$ ,  $0.95 \pm 0.28$  and  $0.91 \pm 0.23$   $\mu m$  respectively.

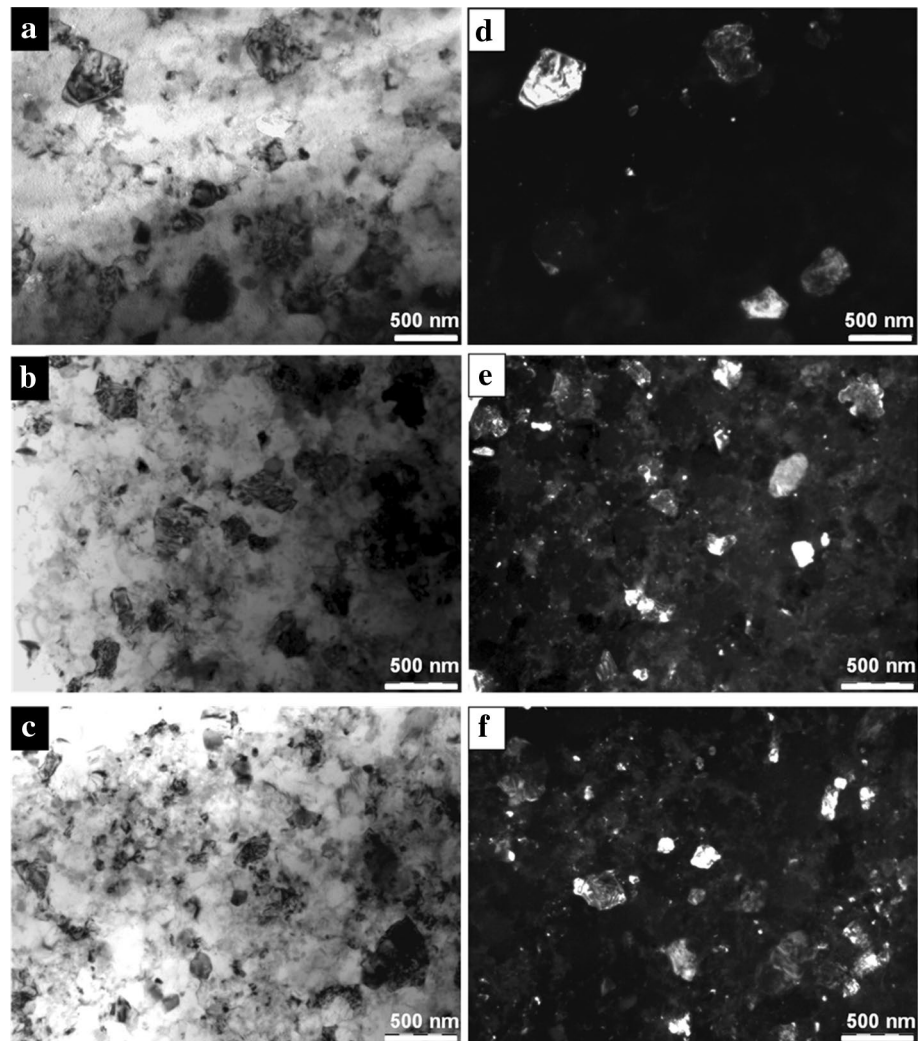
From the grain size analysis, it is further verified that there is no difference in grain size of AA, AC and ANC samples from as-solution treated to peakaged condition.

This is understood as the peakageing temperature (150 °C) used in the study is much lower than the recrystallization temperature of Al alloy and the composites. Therefore, only the microstructures of AA, AC and ANC samples pertaining to the peakaged condition are shown in Fig. 6a–c. TEM dark-field images were utilized for getting well-defined grain boundaries for the apparent estimation of grain size and these images are also shown adjacent to their respective bright-field images, Fig. 7d–f. However, from the as-extruded condition, the grains are observed to be refined further, (Table 2). As it is known, there is a large difference in the value of coefficient of thermal expansion between Al alloy matrix and CNT [3], which led to the punching out of prismatic dislocations due to an abrupt temperature variation that had occurred during quenching [35, 38]. During this process, the dislocations generated rearrange themselves to form finer grains. ANC samples exhibited least average grain size amongst other samples used in the study.

It is also reported by many researchers that the grains refine with the dispersion of CNT in Al alloy [30, 33, 39, 40]. By the examination of microstructures of AA, AC and ANC at each stage of processing carried out in this study i.e., hot pressing, extrusion, solution treated and peakaged conditions, it can be clearly stated that CNT as well as Ni coated CNT have a significant role in refining the microstructure. In order to understand the means by which Ni coated CNT help in refining the grains, TEM analysis was carried out on ANC sample at higher magnification, and the images are shown in Fig. 8a–c. From the figures, it is clear that carbon nanotubes

**Fig. 6** Optical images showing the microstructures after hot pressing: **a** AA, **b** AC and **c** ANC; after hot extrusion: **d** AA, **e** AC and **f** ANC

**Fig. 7** TEM micrographs of samples in peak aged condition: bright-field images **a** AA, **b** AC and **c** ANC; dark-field images: **d** AA, **e** AC and **f** ANC



occupied at the grain boundaries as well as grain interiors, which act as pinning agents preventing the coarsening of grains even at 500 °C during consolidation. The fraction of CNT occupying at the grain boundaries is found to be more in the case of ANC sample (Fig. 8c) suggesting the relatively higher refinement of grains in ANC when compared to AC sample, Table 2.

X-ray diffraction patterns of AA, AC and ANC samples in peak aged condition are given in Fig. 9. It is observed that all the samples exhibited  $\text{CuAl}_2$  and  $\text{Al}_2\text{O}_3$  peaks in addition to high intensity Al peaks. The precipitation of  $\text{CuAl}_2$  phase is well-known during peak ageing of Al alloys (Al–4.4Cu–0.5Mg); whereas,  $\text{Al}_2\text{O}_3$  phase is expected to form due to oxygen content in the as-received Al powder as well as oxygen pick-up during milling owing to the higher chemical affinity of Al with oxygen [1, 4, 5]. In AC sample,  $\text{Al}_4\text{C}_3$  peaks are also present which was already reported very well [7, 8, 18]. The formation of  $\text{Al}_7\text{Cu}_4\text{Ni}$  phase is a noticeable observation in ANC when compared to AA and AC samples (Fig. 9). Even though, the solubility of Ni in Al

is limited by the thermodynamics ( $\approx 0.05\%$ ) [1, 24, 41], it is reported that the processing by MM helps to extend the solid solubility to higher weight fractions [27]. Moreover, Cu is also in the solid solution of Al. Hence, it is reasonable to deduce that the dissolved Ni and Cu in Al lattice precipitate as  $\text{Al}_7\text{Cu}_4\text{Ni}$  phase upon exposure to high temperature during consolidation. The presence of  $\text{Al}_7\text{Cu}_4\text{Ni}$  phase is commonly found in cast Al–Si alloys as well [42, 43]. Another observation is that the fraction of  $\text{CuAl}_2$  phase is less in ANC as compared to other samples. This is attributed to the consumption of some amount of Cu atoms towards the formation of  $\text{Al}_7\text{Cu}_4\text{Ni}$  phase, and hence reduced Cu atoms available for  $\text{CuAl}_2$  precipitation. It may be noted that no characteristic peaks corresponding to  $\text{Al}_2\text{CuMg}$  (*S or S'*) phase was found in XRD patterns of all the samples.

As discussed above,  $\text{CuAl}_2$  phase is found in all the cases. To comprehend the size and its distribution, shape and structure of the precipitates present, TEM bright-field images of AA, AC and ANC samples in peak aged condition, as shown in Fig. 10a–c, were utilized. The  $\text{CuAl}_2$  precipitates, which

**Fig. 8** TEM images of ANC sample showing CNT (dotted circles): **a** at the grain boundary (GB), **b** grain interiors and **c** at both grain boundaries and grain interiors

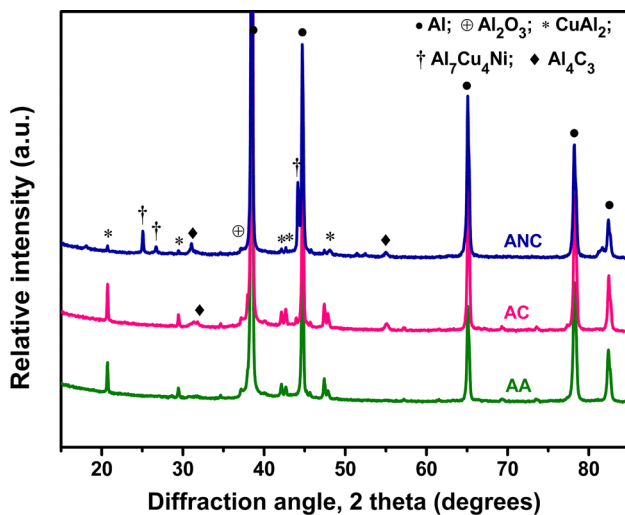
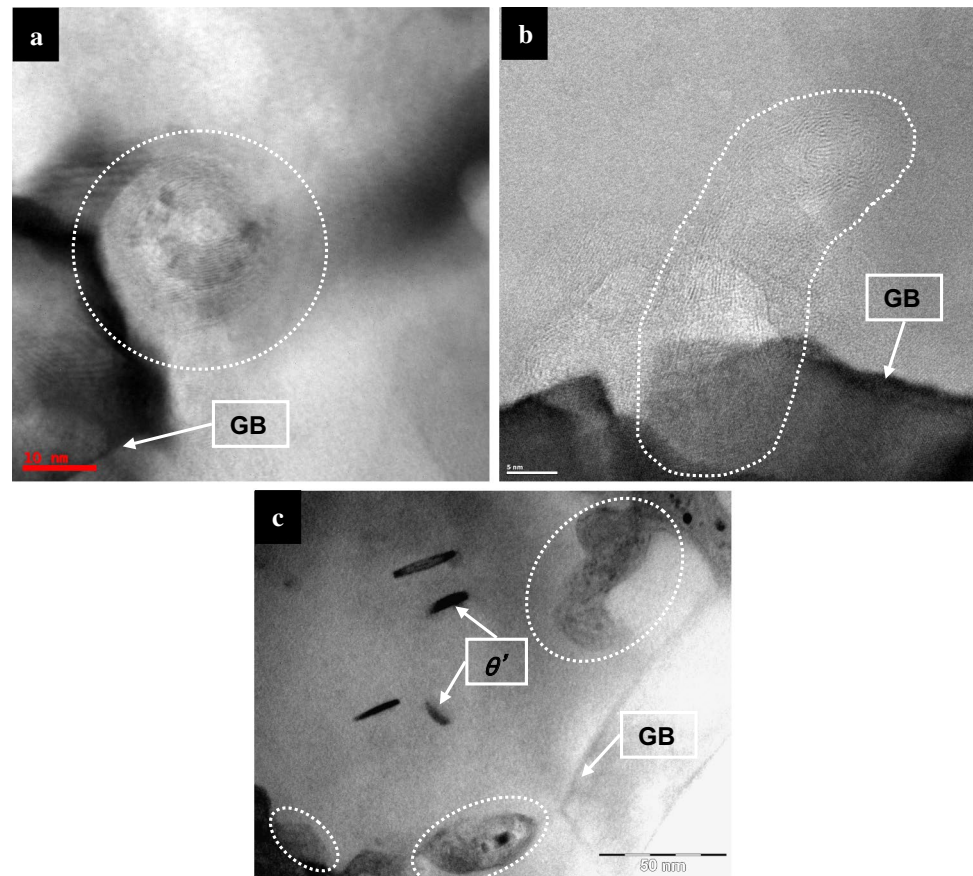


**Fig. 9** XRD patterns of AA, AC and ANC samples in peakaged condition

were confirmed using selected area electron diffraction (SAED) patterns, are of platelet-shaped and their crystal structure is found to match with body-centered tetragonal structure that corresponds to  $\theta'$  (meta-stable  $\text{CuAl}_2$ ) precipitates [44, 45]. However, SAED patterns of all the samples

did not show diffraction spots corresponding to  $S$  or  $S'$  phase; even though finer laths of  $S'$  phase are observed only in AA sample, Fig. 10a. The estimated length and width of these precipitates of AA, AC and ANC samples are provided in Table 3.

From the Table 3, it is clear that the average size of  $\theta'$  precipitates is higher and the number density ( $ND$ ) and volume fraction ( $f_v$ ) of  $\theta'$  precipitates are lower for CNT and Ni coated CNT-dispersed Al alloys (AC and ANC) than the corresponding CNT-free Al alloy (AA) sample. Three possibilities rationalize the above observations: (1) presence of ultrafine grains (2) generation of extra-dislocations and (3) reduced quenched-in vacancies. It is well-known that the vacancies promote diffusion of atoms, and dislocations and grain boundaries act as preferential sites for the nucleation of precipitates [46–50]. It is reported that CNT in Al matrix induces additional dislocations owing to the large difference in the value of coefficient of thermal expansion between Al matrix ( $\alpha_{Al} = 23.6 \times 10^{-6} \text{ K}^{-1}$ ) and CNT ( $\alpha_{CNT} = 1 \times 10^{-6} \text{ K}^{-1}$ ) [3, 34, 51]. Hence, the presence of comparatively finer grains (larger grain boundary area) and more number of dislocations (Table 2) exhibited by AC and ANC samples result in more number of nucleation sites, thereby promoting the kinetics of precipitation. As all the samples have undergone identical peak ageing treatment,



**Fig. 10** TEM images of samples in peakaged condition: **a** AA, **b** AC and **c** ANC. The  $\theta'$  precipitates are identified from respective SAED patterns.  $S'$  precipitate observed in AA sample is also marked

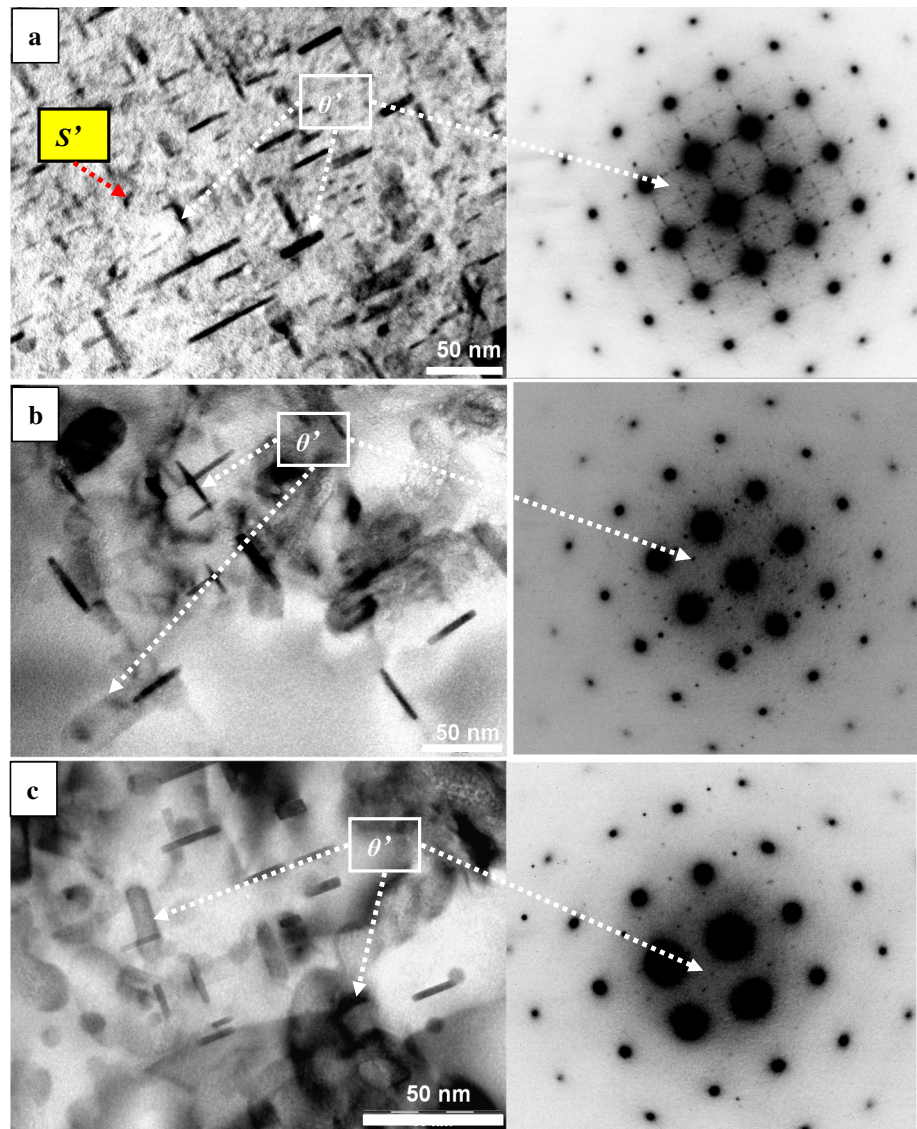


**Table 3** Microstructural and  $\theta'$  precipitate characteristics of AA, AC and ANC samples

Sample ID	Average grain size (nm)	Average precipitate length, $L_p$ (nm)	Average precipitate thickness, $t_p$ (nm)	Number density $\times 10^{22} \text{ m}^{-3}$	Volume fraction, $f_v$	Dislocation density $\times 10^{14} \text{ m}^{-2}$
AA	$336 \pm 60$	$18.79 \pm 8.36$	$3.87 \pm 1.52$	$1.34 \pm 0.2$	$0.0189 \pm 0.008$	3.16885
AC	$225 \pm 74$	$24.71 \pm 9.66$	$5.71 \pm 2.3$	$0.58 \pm 0.23$	$0.0069 \pm 0.0005$	4.48261
ANC	$172 \pm 66$	$20.15 \pm 9.7$	$5.07 \pm 1.86$	$0.34 \pm 0.3$	$0.0053 \pm 0.002$	4.901

the precipitation in AC and ANC has completed in less time and the precipitate particles coarsened during the remaining time of exposure to peak ageing temperature. This resulted in higher particle size and reduction in  $ND$  in AC and ANC samples. The observation of an improved precipitation kinetics in Al-4Cu- $x$  vol% CNT composites ( $x=2, 4$ ) when compared to Al-4Cu alloy was also reported by Nam et al. [34]

in which the  $\theta'$  phase is precipitated after ageing at 130 °C for 72 h in Al alloy, while the precipitation is completed in 24 and 12 h of ageing (at 130 °C) in 2 and 4 vol% CNT-dispersed Al alloy composites respectively. In addition, the lower  $f_v$  of precipitates in AC and ANC samples (Fig. 9b–c) is due to the reduced quenched-in vacancies because of the formation of  $\text{Al}_4\text{C}_3$  and  $\text{Al}_7\text{Cu}_4\text{Ni}$  phases in AC and ANC

samples thereby reducing the diffusion kinetics of the solute atoms. A similar observation was also found by Ceresara et al. [52] where the GP zones formation during aging in Al alloy (Al 601 AB) is suppressed by the oxides of Al and Mg due to low quenched-in vacancies. The relatively lower  $ND$  and  $f_v$  of  $\theta'$  precipitates in ANC sample when compared to AC is due to the utilization of Cu atoms for the formation of particles of  $Al_7Cu_4Ni$  phase.

Average hardness for AA, AC and ANC samples in peak aged condition are provided in Fig. 11. It is observed that the hardness increased with the dispersion of CNT and/or Ni coated CNT in Al alloy. The improvement in hardness for AC and ANC is found to be 18 and 28% respectively. As evident from the microstructures provided in Fig. 7, it can be construed that the presence of much finer grains and hence, more grain boundaries offer more obstructions to the motion of dislocations resulting in higher hardness in AC and ANC samples as compared to AA [53, 54]. In addition, the existence of CNT and  $Al_4C_3$  particles in both AC and ANC samples act as dispersoids leading to the dispersion strengthening [18, 51]. The slightly higher hardness observed in ANC compared to AC sample can be attributed to the presence of an additional  $Al_7Cu_4Ni$  phase.

Engineering stress–strain curves of AA, AC and ANC samples in peak aged condition are shown in Fig. 12. Different deformation characteristics were observed in these samples. The stress–strain curve of AA exhibited similar behaviour as the typical wrought/cast Al alloys. On the other hand, with the dispersion of CNT in Al alloy (AC sample): (a) the flow stress is found to increase with simultaneous reduction in ductility, (b) the work hardening rate is observed to increase at lower strains and then decreased thereafter and (c) the flow stress slightly dropped and deformation continued at a lower stress. The increased work hardening

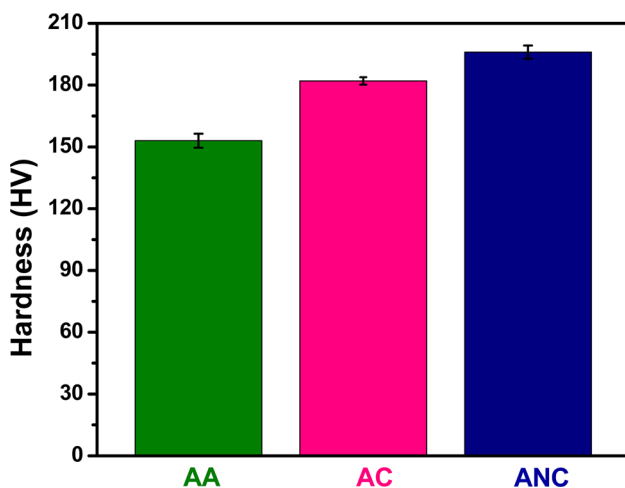


Fig. 11 Hardness of AA, AC and ANC samples in peak aged condition

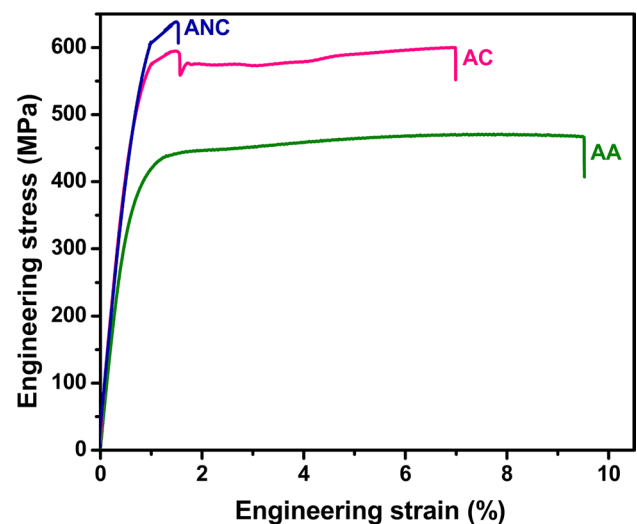


Fig. 12 Engineering stress–strain curves of AA, AC and ANC samples

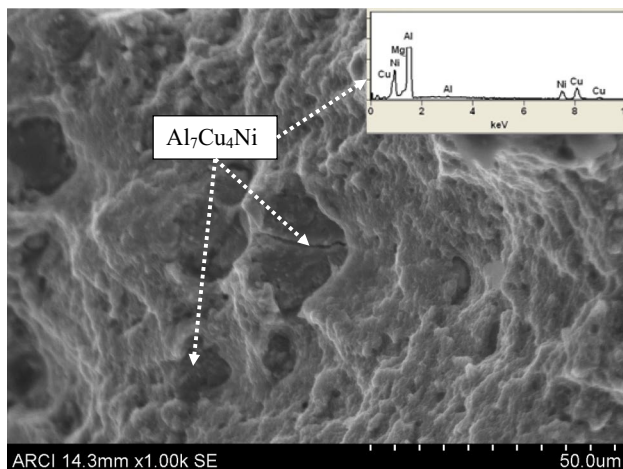
rate at lower strains can be thought of due to the increase in the generation of geometrically necessary dislocations in the presence of ultrafine grains. However, after reaching the ultimate tensile strength (UTS), the flow stress dropped by 6%, but eventually continued at a 3.5% lower stress than UTS. This dropping down of flow stress and the continued deformation could be attributed to the strain softening due to the annihilation of statistically stored dislocations assisted by the ultra-fine grains present in the sample [55]. This observation of strain softening is also reported in other Al alloys viz. Al5083, Al7075, etc. [20, 56, 57]. Furthermore, in the case of ANC sample the characteristics (b) and (c) mentioned above are not fully occurred i.e., there was no continued plastic deformation by ANC, as the sample fractured immediately after reaching the UTS.

The tensile properties like yield and ultimate tensile strengths, and Young's modulus were quantified. The percentage improvement of these properties is provided in Table 4. As with hardness, a concurrent improvement in yield and ultimate tensile strengths, and Young's modulus was observed in CNT/Ni coated CNT-reinforced Al alloy samples.

Even though, the strength and hardness of AC and ANC are enhanced when compared to AA sample (as mentioned above), the ductility is found to decrease in both AC and ANC samples. As it is known that although the dispersoids improve the strength of the material, they also reported to reduce the ductility [46], similar to the case with AC and ANC samples in this study. However, the strain to fracture exhibited by ANC sample is drastically low. The surprisingly reduced ductility in ANC sample is examined by carrying out fractography of the respective tensile specimen and is shown in Fig. 13. From the figure, it is clear that

**Table 4** Mechanical properties of AA, AC and ANC samples in peakaged condition

Sample ID	Hardness (HV)		Yield strength (MPa)		Ultimate tensile strength (MPa)		Young's modulus (GPa)	
	Value	% increase	Value	% increase	Value	% increase	Value	% increase
AA	153	–	380	–	464	–	72	–
AC	181	18	457	20	600	29	89	24
ANC	196	28	567	49	638	38	93	29

**Fig. 13** Fractograph taken from tensile fractured ANC sample. The EDS spectrum of the particle is given as an inset of the figure

fracture occurred due to cracking of some particles, which were confirmed to be  $\text{Al}_7\text{Cu}_4\text{Ni}$  by XRD (Fig. 9) as well as by EDS (inset of Fig. 13). Hence, it can be inferred that  $\text{Al}_7\text{Cu}_4\text{Ni}$  particles act as stress concentration points by nucleating the voids and their coalescence and eventually leading to the fracture of ANC sample.

## 4 Conclusions

The conclusions made from the investigation of the effect of CNT and Ni coated CNT dispersion in Al alloy (AA, Al–4.4Cu–0.5Mg) fabricated through high energy ball milling followed by hot extrusion are as follows:

- The particle size of milled powders was found to decrease with CNT and Ni coated CNT addition due to the retardation of cold welding.
- Formation of  $\text{Al}_4\text{C}_3$  phase was found even in milled Al alloy–Ni coated CNT (ANC) composite powder due to the chemical reaction of Al alloy matrix and CNT at the defects left over on the surface of CNT owing to the diffusion of Ni into the Al lattice.

- Pinning of grain boundaries and grain interiors by CNT and Ni coated CNT aided in preventing grain coarsening in Al alloy–CNT (AC) and ANC samples.
- Strength levels are found to be significantly enhanced for AC and ANC samples when compared to AA because of grain refinement, dislocation and dispersion strengthening mechanisms by CNT,  $\text{Al}_4\text{C}_3$  and  $\text{Al}_7\text{Cu}_4\text{Ni}$  particles.
- The reduction in ductility was marginal for AC samples and considerable for ANC sample. The significant reduction in ductility of ANC sample is due to the presence of  $\text{Al}_7\text{Cu}_4\text{Ni}$  particles which acted as crack initiation points leading to the premature fracture.

**Acknowledgements** Authors would like to thank for the financial aid provided by the ‘Nanomission’ project (Grant No: SR/NM/NS–102011G), under Department of Science and Technology, Government of India.

## References

1. J.R. Davis, *Aluminum and Aluminum alloys*, ASM International Handbook Committee (ASM International, Materials Park, OH, USA, 1993)
2. I. Polmear, D. St. John, J.-F. Nie, M. Qian, in *Light Alloys: Metallurgy of the Light Metals*, 5th edn. (Butterworth-Heinemann, Boston, 2017), pp. 1–29
3. A. Agarwal, S. Bakshi, D. Lahiri, *Carbon Nanotubes: Reinforced Metal Matrix Composites*, 1st edn. (CRC Press, Boca Raton, FL, 2011)
4. J.S. Benjamin, M.J. Bomford, *Metall. Trans. A* **8A**, 1301 (1977)
5. P.S. Gilman, W.D. Nix, *Metall. Trans. A* **12**, 813 (1981)
6. M.M.J. Treacy, T.W. Ebbesen, J.M. Gibson, *Nature* **381**, 678 (1996)
7. H. Kwon, M. Estili, K. Takagi, T. Miyazaki, A. Kawasaki, *Carbon N. Y.* **47**, 570 (2003)
8. C.N. He, N.Q. Zhao, C.S. Shi, S.Z. Song, *J. Alloys Compd.* **487**, 258 (2009)
9. R. Pérez-Bustamante, J.L. Bueno-Escobedo, J. Jiménez-Lobato, I. Estrada-Guel, M. Miki-Yoshida, L. Licea-Jiménez, R. Martínez-Sánchez, *Wear* **292–293**, 169 (2012)
10. H.J. Choi, J.H. Shin, D.H. Bae, *Compos. Sci. Technol.* **71**, 1699 (2011)
11. M.M.H. Bastwros, A.M.K. Esawi, A. Wifi, *Wear* **307**, 164 (2013)
12. S.R. Bakshi, A. Agarwal, *Carbon N. Y.* **49**, 533 (2011)
13. C. He, N. Zhao, C. Shi, X. Du, J. Li, H. Li, Q. Cui, *Adv. Mater.* **19**, 1128 (2007)
14. M. Jagannatham, S. Sankaran, P. Haridoss, *Mater. Sci. Eng. A* **638**, 197 (2015)

15. A. Maqbool, M.A. Hussain, F.A. Khalid, N. Bakhsh, A. Hussain, M.H. Kim, *Mater. Charact.* **86**, 39 (2013)
16. O. Carvalho, M. Buciumeanu, D. Soares, F.S. Silva, G. Miranda, *J. Mater. Eng. Perform.* **24**, 2535 (2015)
17. O. Carvalho, M. Buciumeanu, S. Madeira, G. Miranda, F.S. Silva, *Compos. Part B Eng.* **93**, 229 (2016)
18. N.S. Anas, R.K. Dash, T.N. Rao, R. Vijay, *J. Mater. Eng. Perform.* **26**, 3376 (2017)
19. N.S. Anas, S.B. Chandrasekhar, R.K. Dash, Tata N. Rao, R. Vijay, *Trans. Indian. Inst. Met.* (2019). <https://doi.org/10.1007/s12666-019-01736-7>
20. K. Ma, H. Wen, T. Hu, T.D. Topping, D. Isheim, D.N. Seidman, E.J. Lavernia, J.M. Schoenung, *Acta Mater.* **62**, 141 (2014)
21. G.K. Williamson, W.H. Hall, *Acta Metall.* **1**, 22 (1953)
22. G. Liu, G.J. Zhang, X.D. Ding, J. Sun, K.H. Chen, *Mater. Sci. Eng. A* **344**, 113 (2003)
23. L. Pauling, *J. Am. Chem. Soc.* **69**, 542 (1947)
24. B. Predel, in *Ac-Au – Au-Zr*, ed. by O. Madelung (Springer, Berlin, 1991), pp. 1–7
25. J.S. Benjamin, T.E. Volin, *Metall. Trans.* **5**, 1929 (1974)
26. A. Canakci, S. Ozsahin, T. Varol, *Powder Technol.* **228**, 26 (2012)
27. C. Suryanarayana, *Prog. Mater. Sci.* **46**, 1–184 (2001)
28. R. Pérez-Bustamante, F. Pérez-Bustamante, I. Estrada-Guel, L. Licea-Jiménez, M. Miki-Yoshida, R. Martínez-Sánchez, *Mater. Charact.* **75**, 13 (2013)
29. X. Zhu, Y.G. Zhao, M. Wu, H.Y. Wang, Q.C. Jiang, *J. Alloys Compd.* **674**, 145 (2016)
30. F. Mokdad, D.L. Chen, Z.Y. Liu, B.L. Xiao, D.R. Ni, Z.Y. Ma, *Carbon N. Y.* **104**, 64 (2016)
31. H.J. Choi, J.H. Shin, D.H. Bae, *Compos. Part A Appl. Sci. Manuf.* **43**, 1061 (2012)
32. R. Pérez-Bustamante, I. Estrada-Guel, P. Amézaga-Madrid, M. Miki-Yoshida, J.M. Herrera-Ramírez, R. Martínez-Sánchez, *J. Alloys Compd.* **495**, 399 (2010)
33. C.F. Deng, D.Z. Wang, X.X. Zhang, A.B. Li, *Mater. Sci. Eng. A* **444**, 138 (2007)
34. D.H. Nam, Y.K. Kim, S.I. Cha, S.H. Hong, *Carbon N. Y.* **50**, 4809 (2012)
35. N.S. Anas, M. Ramakrishna, R.K. Dash, Tata N. Rao, R. Vijay, *Mater. Sci. Eng.: A* **751**, 171–182 (2019)
36. M. Lewandowska, H. Garbacz, W. Pachla, A. Mazur, K.J. Kurzydłowski, *Mater. Sci.* **23**, 279 (2005)
37. Y. Estrin, A. Vinogradov, *Acta Mater.* **61**, 782 (2013)
38. A. Eikum, G. Thomas, *Acta Metall.* **12**, 537 (1964)
39. D.H. Nam, S.I. Cha, B.K. Lim, H.M. Park, D.S. Han, S.H. Hong, *Carbon N. Y.* **50**, 2417 (2012)
40. Z.Y. Liu, B.L. Xiao, W.G. Wang, Z.Y. Ma, *Carbon N. Y.* **69**, 264 (2014)
41. H. Okamoto, *J. Phase Equilib.* **14**, 257 (1993)
42. Y. Yang, K. Yu, Y. Li, D. Zhao, X. Liu, *Mater. Des.* **33**, 220 (2012)
43. Y. Li, Y. Yang, Y. Wu, L. Wang, X. Liu, *Mater. Sci. Eng. A* **527**, 7132 (2010)
44. S.P. Ringer, K. Hono, *Mater. Charact.* **44**, 101 (2000)
45. S.C. Wang, M.J. Starink, N. Gao, *Scr. Mater.* **54**, 287 (2006)
46. W.D. Callister, *Fundamentals of Materials Science and Engineering*, 5 edn. (Wiley, Newyork, 2001)
47. G.C. Weatherly, R.B. Nicholson, *Philos. Mag.* **17**, 801 (1968)
48. C. García-Cordovilla, E. Louis, *Metall. Trans. A* **15**, 389 (1984)
49. S.P. Ringer, B.C. Muddle, I.J. Polmear, *Metall. Mater. Trans. A* **26A**, 1659 (1995)
50. A.K. Jena, A.K. Gupta, M.C. Chaturvedi, *Acta Metall.* **37**, 885 (1989)
51. R. George, K.T. Kashyap, R. Rahul, S. Yamdagni, *Scr. Mater.* **53**, 1159 (2005)
52. S. Ceresara, P. Fiorini, *Powder Metall.* **22**, 1 (1979)
53. E.O. Hall, *Proc. Phys. Soc. Sect. B* **64**, 747 (1951)
54. N.J. Petch, *J. Iron Steel Inst.* **174**, 25 (1953)
55. M.A. Meyers, A. Mishra, D.J. Benson, *Prog. Mater. Sci.* **51**, 427 (2006)
56. T.D. Topping, B. Ahn, Y. Li, S.R. Nutt, E.J. Lavernia, *Metall. Mater. Trans. A* **43**, 505 (2012)
57. Z. Zhang, T. Topping, Y. Li, R. Vogt, Y. Zhou, C. Haines, J. Paras, D. Kapoor, J.M. Schoenung, E.J. Lavernia, *Scr. Mater.* **65**, 652 (2011)

**Publisher's Note** Springer Nature remains neutral with regard to jurisdictional claims in published maps and institutional affiliations.